Chemical Etching of Molybdenum Trioxide: A New Tailor-Made Synthesis of MoO_3 Catalysts

H. C. Zeng*

Department of Chemical Engineering, Faculty of Engineering, National University of Singapore, 10 Kent Ridge Crescent, 119260 Singapore

Received October 10, 1997

Crystalline catalysts of orthorhombic MoO_3 have been prepared via a vapor phase deposition method, and their crystallographic structure has been affirmed by XRD and FTIR investigations. A chemical etching method has been developed for restructuring these thermally processed catalysts. Using a 0.1 M NaOH etchant, {001} and {100} plane areas of the catalysts can be significantly increased while surface steps, ledges, and terraces are created. Moreover, alternate crystal plane combinations of either {100} and {010} or the {001} and {010} are observed on crystal edges and rectangular etch pits in the basal planes {010}. Both materials chemistry of MoO_3 and etching mechanisms have been studied on the basis of the surface morphological evolution of etching patterns of the catalysts. Technological merits and the processing parameters of this new method have also been identified. Following the findings of the current work, it is believed that the chemically carved surface structures may be crucial for certain MoO_3-involving catalytic reactions.

I. Introduction

Molybdenum trioxide (MoO_3) is one of the most widely used catalysts today in heterogeneous catalysis. Its vastly covered applications include molecular hydrogenation, oxidative dehydrogenation, epoxidation, isomerization, disproportionation, polymerization, etherification, addition, and dehydrogenation.[1−5] To increase its working efficiency in actual chemical processes, MoO_3 is commonly supported on a porous, high surface area "inert" carrier such as Al_2O_3 or MgO using the conventional impregnation method. In many cases, the isolated polyhedra or thin layers of MoO_3 are dispersed at the surface of carriers due to limited miscibility between molybdenum compounds and supporting substrates at pretreatment temperatures.

When it crystallizes, MoO_3 forms hexagonal or rectangular platelets. The ⟨100⟩ dimension of the latter platelets has been known to be from a few tens of micrometers to submicron in scale.[3,6] The thermodynamically stable phase is favored as the following hierarchy: amorphous MoO_3 < monoclinic MoO_3 (β, hexagonal) < orthorhombic MoO_3 (α, rectangular).[7,8] For example, the orthorhombic phase has been reported to be stable at 300 °C in the evaporative preparation of MoO_3.[7] Because the reaction temperature used in many chemical processes exceeds 300 °C, high thermal stability of the MoO_3 catalysts is required in addition to high surface area or dispersity of the active component, a prerequisite for a practical catalyst.

To improve catalyst performance, endeavors in the fabrication of large surface area or low bulk density MoO_3 materials have been made for many decades.[9,10] For example, in addition to the low-density MoO_3 prepared by sublimation and ultrafine particle MoO_3 (70 nm) by arc vaporization,[9] ultrafine particle MoO_3 has been recently prepared by the low-temperature sol−gel route.[10] However, due to thermal aggregation, these unsupported sol−gel-derived xerogels or aerogels have poor thermal stability upon heat treatment, although their as-prepared surface areas are comparable with the supported one.[10]

It is noted that recent advances in catalytic materials take a much closer look not only at the chemical and physical phenomena at the catalyst/carrier interface but also at the more detailed structural and crystalline features of both components. It is also noted that the knowledge and experience of researchers in ceramic and electronic materials are having a profound impact on the fundamental understanding of the new types of catalyst processing. Regarding the MoO_3 catalysts, clearly, there is an urgent need to develop a newer catalyst preparation method or modification aiming at both high surface area and thermal stability. As high surface area and thermal stability of the MoO_3 have been achieved in the MoO_3/Al_2O_3 system using the impregnation method, the current paper will explore the possibility of further increases in surface area and alteration of crystallographic planes of the orthorhombic MoO_3. In particular, we will apply a chemical etching method, which has been used in inorganic single-crystal investigation,[11,12] to the current

* Tel.: +65 874 2896. Fax: +65 779 1936. E-mail: chezhc@nus.edu.sg.

(1) Haber, J. In *Molybdenum: An Outline of Its Chemistry and Uses*; Braithwaite, E. R.; Haber, J., Eds.; Elsevier Science: Amsterdam, 1994; Chapter 10, p 479.
(2) Sabu, K. R.; Rao, K. V.; Nair, C. G. R. *Indian J. Chem.* **1994**, *33B*, 1053.
(3) Zhang, C.-M.; Chen, S.-Y.; Yang, Z.-P.; Peng, S.-Y. In *Sol−Gel Processing and Applications*; Attia, Y. A., Ed.; Plenum Press: New York, 1994; p 379.
(4) Hayashi, H.; Sugiyama, S.; Masaoka, N.; Shigemoto, N. *Ind. Eng. Chem. Res.* **1995,** *34*, 137.
(5) Fournier, M.; Aouissi, A.; Rocchiccioli-Deltcheff, C. *J. Chem. Soc., Chem. Commun.* **1994** (3), 307.
(6) Eda, K. *J. Solid State Chem.* **1991**, *95*, 64.
(7) Julien, C.; Khelfa, A.; Hussain, O. M.; Nazri, G. A. *J. Cryst. Growth* **1995**, *156*, 235.
(8) Nazri, G. A.; Julien, C. *Solid State Ionics* **1992**, *53−56*, 376.
(9) Tsigdinos, G. A.; Swanson, W. W. *Ind. Eng. Chem. Prod. Res. Dev.* **1978**, *17*, 208.
(10) Zhang, C.-M.; Chen, S.-Y.; Xu, D.-P.; Peng, S.-Y. In *Sol−Gel Processing and Applications*; Attia, Y. A., Ed.; Plenum Press: New York, 1994; p 73.
(11) Zeng, H. C. *J. Cryst. Growth* **1996**, *160*, 119.
(12) Zeng, H. C. *J. Cryst. Growth* **1997**, *171*, 136.

S0020-1669(97)01269-X CCC: $15.00
Published on Web 04/01/1998

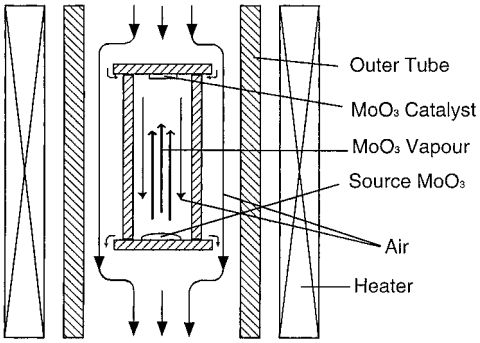

Figure 1. Experimental setup used in the current study for catalyst preparation. Note that the air can travel through interspacing between quartz plate and inner tube.

catalyst research. Because the rectangular crystallites of MoO_3 (orthorhombic) are commonly observed in the catalysts after calcination, as mentioned earlier, this etching study will examine the chemical reactivity between the crystalline MoO_3 and a NaOH etchant. Furthermore, the effects of this new fabrication method, which creates a larger surface area and a more complex surface structure for MoO_3, will be discussed in relation to the chemistry of this catalytic compound.

II. Experimental Section

Crystalline MoO_3 catalysts were prepared in a wall-heated sublimation apparatus situated in a vertical electric furnace (Carbolite, Figure 1). The preparation compartment comprises an inner quartz tube and two square plates made of the same material. The compartment tube was further enclosed in a larger quartz tube to control growth atmosphere. A sample preparation procedure can be described as follows. Briefly, 50−100 mg of MoO_3 powder (as-purchased MoO_3, purity 99.5%, Aldrich Chemical Co.) was loaded onto the bottom quartz plate in each experiment, as depicted in Figure 1. The top plate was located near the furnace end, and its temperature was lower. Due to the temperature gradient (∼11−13 °C/cm) between the two plates, the sublimed MoO_3 was condensed on the top plate of the growth compartment. Temperatures of source and growth zones were monitored with a K-type thermocouple. The preparation background gas (purified compressed air) was introduced to the sublimation from the top of external tube to the upper quartz plate at a flow rate of 0.87−20.0 dm^3/h. The air is introduced to ensure a sufficient oxygen supply to the MoO_3 formation and thus the correct stoichiometry of the compound. The nutrient MoO_3 powder was heated at a constant temperature (in 677−702 °C range) for various sublimation times (2−16 h).

Crystallographic information of the as-prepared MoO_3 catalysts was established with the powder X-ray diffraction (XRD). The diffraction intensity−2θ theta spectra were measured in a Shimadzu XD-D1 using an X-ray generator operated at 35 kV/30 mA with Cu Kα radiation (λ = 1.5418 Å) at a scanning rate of 4° min^{-1}. Furthermore, Mo−O bonding situations of the samples were investigated with Fourier transform infrared spectroscopy (FTIR).[13−16] Using the KBr pellet technique, the FTIR spectra of the samples were recorded with 4 cm^{-1} resolution on a computerized FTIR spectrometer (Shimadzu FTIR-8001). The MoO_3:KBr ratio was optimized according to the general approach that the strongest bands should have intensities in the transmission range 5−15%. Forty scans were performed for each spectrum to obtain a good signal:noise ratio. Chemical etching study was carried out at room temperature with a 0.1 M NaOH aqueous solution. Typically, a suitable MoO_3 crystallite was selected and placed on a clean microscope glass slide. Before the etching process, the original surface morphology of the sample was preexamined with an optical microscope (Olympus BH-2) and its micrograph was taken. A drop or two of NaOH etchant was then added to the sample, and the time was recorded. After a desired period of time, deionized water was flooded extravagantly to the sample to terminate the etching. The etched sample was then air-dried and investigated again under the microscope for its etching morphology. It is noted that there was no sign of amorphous materials existing on the surface after water rinsing. Sequential etching of the same piece of the sample was further performed with a recorded time interval. All micrographs in morphological study were taken perpendicular to the ⟨010⟩ direction of the crystal.

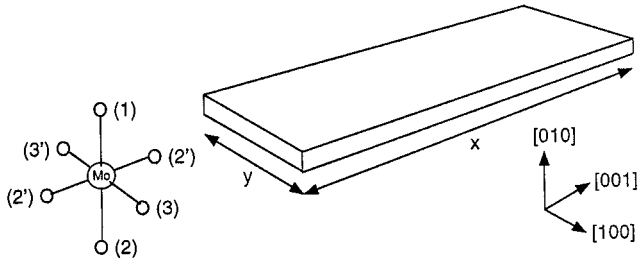

Figure 2. Crystallographic orientation of the orthorhombic MoO_3 and molecular structure of a MoO_6 unit in the crystal lattice. Bond length data:[1] Mo−O(1) = 1.67 Å, Mo−O(2) = 2.33 Å, Mo−O(2′) = 1.95 Å, Mo−O(3) = 1.73 Å, and Mo−O(3′) = 2.25 Å.

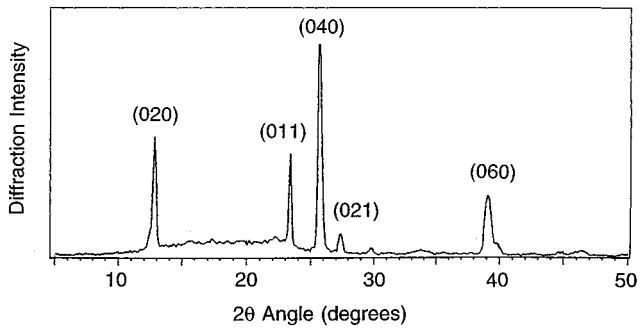

Figure 3. XRD spectrum of powder sample of the as-prepared orthorhombic MoO_3 catalyst.

III. Results

1. Metal Oxide Characterization. Crystallites of MoO_3 prepared in the current work give a rectangular morphology as shown in Figure 2. In particular, the ⟨100⟩ dimension of the crystallites ranges from 250 μm to submicron in scale. An XRD spectrum for as-grown crystalline MoO_3 powder is reported in Figure 3, which indicates that the crystallographic structure of the catalyst is orthorhombic (α-MoO_3). The (0k0) peaks, with k = 2, 4, 6, are much stronger than those of (011) and (021) peaks. Referring to the schematic drawing the α-MoO_3 structure shown in Figure 2, the above observation reveals a predominant two-dimensional growth of the crystallites along the basal planes of {010} of α-MoO_3 when the MoO_3 vapor (in the forms of cluster molecules Mo_3O_9, Mo_4O_{12}, and Mo_5O_{15}[17]) is condensed.

The resulting sheetlike MoO_3 is further investigated with FTIR, the spectrum of which is displayed in Figure 4. A number of Mo−O stretching modes can be identified from this spectrum, which are in good agreement with the literature data for the layered α-MoO_3.[6,7,17] Due to the longitudinal transverse splitting effect,[6] the IR bands are influenced in their peak position and bandwidth by crystallite size and morphology in the KBr pellet sample. In the low-wavenumber region, a large shoulder band

(13) Zeng, H. C.; Qian, M. *J. Mater. Chem.* **1996**, *6*, 435.
(14) Qian, M.; Zeng, H. C. *J. Mater. Chem.* **1997**, *7*, 493.
(15) Zeng, H. C.; Tung, S. K. *Chem. Mater.* **1996**, *8*, 2667.
(16) Zeng, H. C.; Sheu, C. W.; Hia, H. C. *Chem. Mater.* **1998**, in press.
(17) Chippindale, A. M.; Cheetham, A. K. In *Molybdenum: An Outline of Its Chemistry and Uses*; Braithwaite, E. R., Haber, J., Eds.; Elsevier Science: Amsterdam, 1994; Chapter 3, p 146.

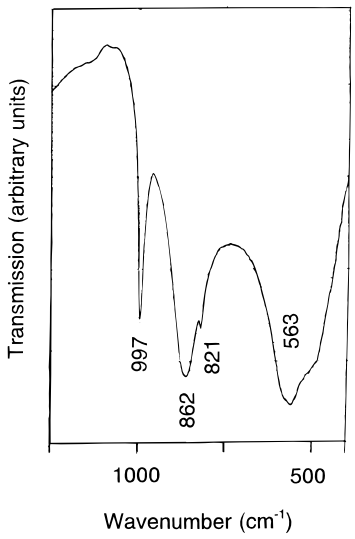

Figure 4. FTIR spectrum of the as-prepared orthorhombic MoO_3 catalyst.

at around 500 cm^{-1} is attributable to the vibration modes of $\nu Mo-O_{(2)}$ B_{3u} and $\nu Mo-O_{(2)}$ B_{2u} between Mo and oxygen between two adjacent sublayers. The band at around 563 cm^{-1} belongs to the $\nu Mo-O_{(2')}$ B_{1u} mode whose Mo and oxygen are located within the same sublayer.[6,8] The large band at ca. 863 cm^{-1} is assigned to Mo and bridge-oxygen vibration ($\nu Mo-O_{(3')}$ B_{3u}) within a sublayer. The peak at 822 cm^{-1}, which is well resolved from the band at 863 cm^{-1}, is also attributed to another mode of Mo and bridge-oxygen in the sublayer ($\nu Mo-O_{(3')}$ B_{2u}).[6,8] Finally, the sharp band at higher wavenumber region (997 cm^{-1}) can be assigned to the basal plane oxygen which contains both $\nu Mo-O_{(1)}$ B_{3u} and $\nu Mo-O_{(1)}$ B_{2u} modes.[6,8]

2. Surface Morphology Evolution. The above structural analyses confirm that the layered α-MoO_3 has been obtained in the sample preparation. In the following, two crystalline α-MoO_3 samples will be studied to explore their surface morphology development when placed with the NaOH etchant.

The etching evolution of the first α-MoO_3 sample is shown in Figure 5a−d. As can be seen, the as-grown crystal is rectangular before etching. There are many terraces parallel to the {100} planes. In addition, curved terraces with no defined natural crystal planes are also visible in Figure 5a. After 20 s of etching (Figure 5b), sample edges of the {100} planes are much rougher than the one along [001], indicating a fast etching rate along the ⟨100⟩ direction. Interestingly, many tiny etch pits can be found along these terraces/ledges, especially along the curved ones. With a longer etching time of 30 s (total accumulated time), the etching in the ⟨100⟩ direction widens further, resolving many new steps etched upon original as-grown parallel terraces which are wavy locally, but overall directions of the etched step are still perpendicular to ⟨100⟩. It should be mentioned that the curved terraces are more active than {100} planes toward the etchant, as they almost disappear after this etching. For example, the U-shaped terraces in the right-hand side of the micrographs (Figure 5a,b) change to the rectangular terraces which are composed {100} and {001} facets. When the crystal is further etched for a total accumulated time of 60 s, the etching results are even more pronounced. Shown in Figure 5d, the etched pits with pyramid structure can now be observed all over the {010} planes, including the newly born {010} terraces. Although the pyramid etch pits are the common morphology on {010}, other features such as the round dark holes should also be noticed.

In Figure 6a−d, chemical etching of the second α-MoO_3 sample will further examined. Different from the previous sample, this crystal has more terraces growing along the ⟨001⟩ directions. After etching for 20 s, round dots on crystal terraces emerge (Figure 6a). These dots are crystal defects that are buried within the terraces. Since they are a secondary phase to a terrace, depletion of these defects is relatively easy, as shown in the subsequent micrographs. With more etching time (total 40 s), it is found that the curved terraces in the ⟨001⟩ direction are straightened to low-angle facets (Figure 6b,c). For instance, as shown at the left-hand side lower part of the micrographs, final chemically inert planes for the curved terraces are indeed {001}. By measuring the distance between a reference point (reversed-side crystal morphology; lighter parts) and the etching fronts in Figure 6a−c, it is also confirmed that the etching rate of terraces along ⟨100⟩ is faster than that along ⟨001⟩. Again, more etching fronts are generated along the crystal side edges, i.e., the {100} faces. In agreement with the observed {100} and {001} planes, pyramids of chemical etch pits for longer etching time (60 s, Figure 6d) are well aligned along the ⟨001⟩ and ⟨100⟩ directions. Due to the fast etching rate in ⟨100⟩, these pyramids are elongated in the ⟨100⟩ direction. Within the rectangular etch pits, {010} platforms are also observable, which reflects again the layered structure of α-MoO_3 in the inner parts, noting that the etchant attacks the crystal three-dimensionally.

3. Three-Dimensional Etchings. On the basis of the above morphological observations, it is possible to draw some general findings. For a rectangular α-MoO_3 crystal, with dimensions of x (length), y (breadth), and z (height), the reduction of volume upon etching in different parts of crystal differs, since the observed etching rate varies. Considering the cases shown in Figure 7a,b for the side plane ({001} and {100}) etchings, one would recognize that the dimension ratio of x_i/y_i is smaller than x_f/y_f (where i and f denote initial and final, respectively) after the chemical etching, since the etching rate in ⟨100⟩ is greater than in ⟨001⟩ which results in $x_i \approx x_f$ and $y_i > y_f$. As this MoO_3 depletion process involves also simultaneous etching on {010} plane, though it is the slowest, the final resulting side planes are no longer flat, as illustrated in Figure 7a,b. Due to the fast rate in the ⟨100⟩ direction, larger naked {010} emerge from the {100} plane etching compared to the one along ⟨001⟩, which has been shown in Figures 5c and Figure 6b,c. On the basis of these results, it can be summarized that the total surface area reduction due to these etchings has the sequence of $\{100\}_{loss} < \{001\}_{loss} < \{010\}_{loss}$, considering the starting crystal dimensions depicted in Figure 2.

In addition to the above "external" etchings, nevertheless, there is an "internal" etching which increases plane areas of both {100} and {001} faces at no consumption of the {010} planes, as schematically shown in Figure 7c,d. This type of etching starts at a defect site on the {010} plane. When it forms, an etch pit (negative volume) expands three-dimensionally in ⟨010⟩, ⟨100⟩, and ⟨001⟩ according to their respective etch rates. Since the pyramid slopes contain the observed etched planes of {001} and {100}, the total areas of the {001} and {100} now are much greater than those without the "internal" etching. In particular, the {001} plane area is increased more than the {100} plane due to the fast etching rate in the ⟨100⟩ direction. Nevertheless, it should be pointed out that the population ratio of {001}:{100} created upon this "internal" etching is a constant, since all the pyramids are similar in shape, i.e., with a similar length/breadth ratio (Figures 5d and 6d). Viewing from the ⟨010⟩ direction, it can be realized that the {010} plane is now divided into many small concentric rectangular platforms and

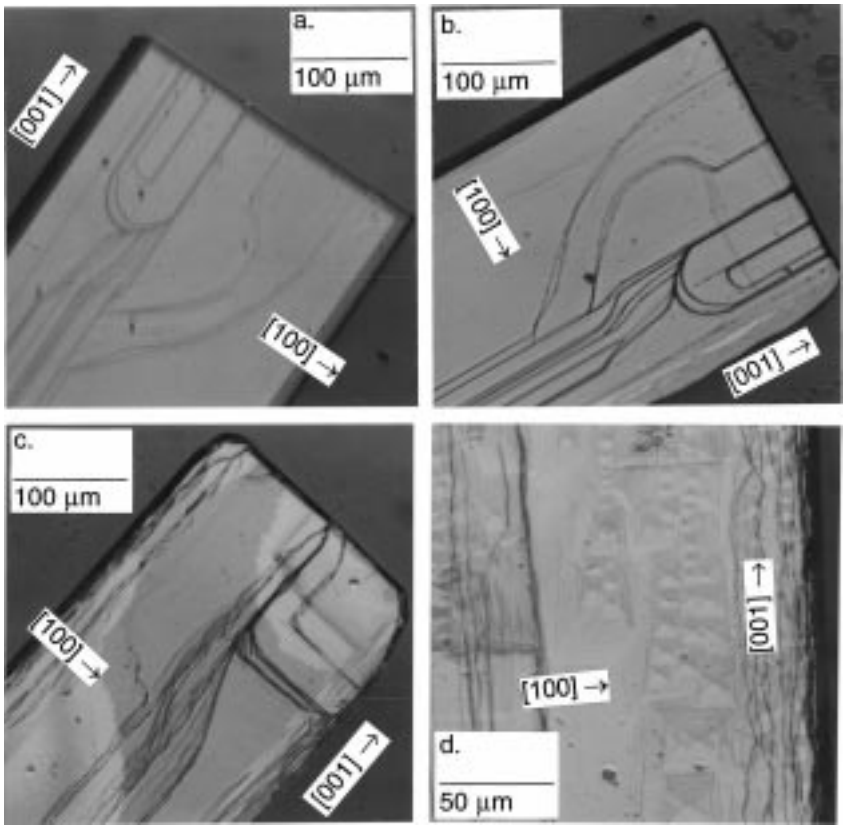

Figure 5. Morphological development of the first sample (see the text) upon chemical etching: (a) before etching (taken from the reverse side of the crystal); (b) 20 s etching; (c) 30 s etching; (d) 60 s etching.

inter-rectangle space (Figures 5d and 6d), but the total area of the {010} is still kept essentially the same as the one without internal etching. Although it is not possible to measure the depth of the etched pits directly with the optical microscope (which can be determined by scanning probe microscopy), the relative dimension ratio of the rectangular edges can be determined rather accurately using the current technique. As lengths of these edges reflect the rates of in-plane ({010}) etching, it is possible to determine the relative etching rate along the ⟨100⟩ and ⟨001⟩. On the basis of the etch pit morphology of Figure 6d, the relative etching rate between ⟨100⟩ and ⟨001⟩ is ca. 1.6, which means that the rate in the ⟨100⟩ direction is about 0.6 times faster than that in ⟨001⟩ .

IV. Discussion

1. Proposed Etching Mechanisms. Microscopically, chemical etching is a chemical reaction between lattice ions and etchant chemical species. In the current case, this chemical reaction can be written below, based on general reactions between MoO_3 and bases:[18]

$$MoO_3 + 2Na^+ + 2OH^- = 2Na^+ + MoO_4^{2-} + H_2O \quad (1)$$

To be more specific, the reaction is a nucleophilic addition of hydroxyl group OH^- to the Mo(VI) cation in the MoO_3 lattice, forming a soluble species of MoO_4^{2-} which leaves the crystalline solid. The etching process can then be viewed as one that breaks a MoO_6 octahedron and forms a MoO_4 tetrahedron (i.e., MoO_4^{2-}), i.e., transforming octahedran to tetrahedron process.

The bonding situations for MoO_6 along the ⟨100⟩ direction are substantially different from the ⟨001⟩, which will result in different chemical reactivities toward the etchant. For an idealized α-MoO_3 crystal, both Mo and O ions on {010} planes are coordinatively saturated. Therefore, in the absence of surface defects, the {010} planes would be chemically inert to the etchant. Nevertheless, both Mo and O ions are unsaturated on {100} planes because the bridge oxide ($O_{(3)}$, Figure 2) is only one-side-coordinated with the Mo(VI), i.e., one of the two bridge oxygens becomes a new type of terminal oxygen on the {100}. Due to this, there are four types of oxygen for a MoO_6 octahedron on the {100} planes: (i) the common oxygen between the sublayers (two $O_{(2')}$ and one $O_{(2)}$); (ii) the remaining bridge oxygen (one $O_{(3')}$); (iii) the original terminal oxygen along ⟨010⟩ axis (one $O_{(1)}$); and (iv) the new terminal oxygen along ⟨100⟩ axis (one $O_{(3)}$). For this surface termination, it had been estimated in the literature that the formal charges on the unsaturated oxygen ($O_{(3)}$) on {100} and on Mo are −1.5 and +1.5, respectively.[19] From this residual charge on Mo(VI), it is understandable that an OH^- is attracted to the chemically unsaturated solid surface. The following shows a proposed etching mechanism on the {100} surface based on the current experimental results and formal charge analysis:[19]

$$MoO_3 + OH^- = H{-}O{-}MoO_3^- \quad (O \text{ in } MoO_3 = O_{(1)}, O_{(2')}, \text{ and } O_{(3)}) \quad (2)$$

$$OH^- + H{-}O{-}MoO_3^- = MoO_4^{2-} + H_2O \quad (3)$$

When it approaches Mo(VI), an OH^- weakens further the

(18) Braithwaite, E. R. In *Molybdenum: An Outline of Its Chemistry and Uses*; Braithwaite, E. R., Haber, J., Eds.; Elsevier Science: Amsterdam, 1994; Chapter 1, p 17.

(19) Haber, J. In *Molybdenum: An Outline of Its Chemistry and Uses*; Braithwaite, E. R., Haber, J., Eds.; Elsevier Science: Amsterdam, 1994; Chapter 10, p 494.

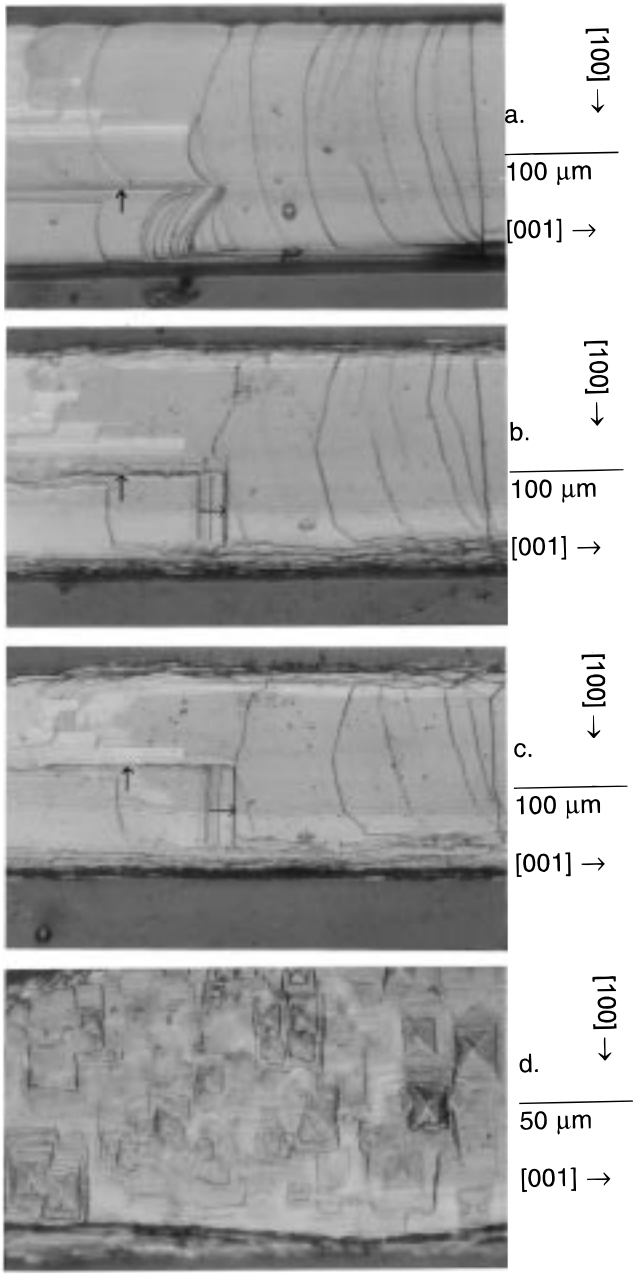

Figure 6. Morphological development of the second sample (see the text) upon chemical etching: (a) 20 s etching; (b) 40 s etching; (c) 60 s etching; and (d) 60 s etching. Arrows indicate the moving directions of the etched planes.

original weaker Mo−O bonds in an octahedron, such as Mo−$O_{(3')}$ and Mo−$O_{(2)}$ (Figure 2). According to chemical stoichiometry of MoO_3, a MoO_4^{2-} takes away only three oxygen atoms from an octahedron if the etching occurs in a one (octahedron) by one fashion. From the energy viewpoint, among the six oxygen atoms, two terminal oxygen ($O_{(1)}$ and $O_{(3)}$) and one of the two common oxygen ($O_{(2')}$) would be taken away since their chemical bondings are the strongest (Mo−O bond lengths are the shortest) compared to the remaining oxygen atoms. When an $O_{(2')}$ is removed along with a MoO_4^{2-}, it leaves behind an unsaturated $O_{(2')}$ and creates more formal charge on Mo(VI) which is in turn more inviting to an OH^-. As the two common oxygen atoms ($O_{(2')}$) are chemically equivalent (Figure 2), it is likely that the etching on the {100} planes adopts a chain-peeling process as described in Figure 8, in which an entire chain of MoO_6 octahedrons can be peeled off sequentially from the plane. As proposed in eq 2, a proton released from surface−solid complex H−O−MoO_3^- will be accepted by another OH^- in the solution, forming a MoO_4^{2-} and a H_2O molecule (eq 3). It is important to point out that the etching postulation is validated with experimental observation that the moving {100} planes are well preserved during the etching (Figures 5 and 6).

For the {001} planes, an additional analogous analysis can be performed. On these surfaces, both the unsaturated oxygen $O_{(2')}$ and Mo are also expected. On the basis of a similar theoretical estimation, the formal charges on Mo(VI) and the unsaturated oxygen ($O_{(2')}$) are +0.779 and −0.779, respectively.[19] Due to the localized positive charge on Mo, an OH^- can now insert into Mo in the nucleophilic attachment, as described in eqs 2 and 3. Since the formal charge on Mo in the current case is not as large as in the previous one ({100} face etching), it is not surprising that the etching rate along ⟨001⟩ is slower (Figures 5 and 6). Furthermore, the chain-peeling mechanism illustrated in Figure 9 can also be proposed, as the {001} planes are well kept in the moving etching fronts (Figures 5 and 6). To confirm these mechanisms, further investigation on etching reactions and etching kinetics will be carried out with atomic force microscopy.

2. Etching and Catalyst Restructuring. In the previous sections, the possibility of the restructuring α-MoO_3 by chemical etching has been demonstrated. This low-temperature basic solution technique clearly changes the transition metal oxide MoO_3 (acidic) in surface termination fashion and thus its interfacial (solid−gas) properties and chemical reactivity in heterogeneous catalysis. Apparently, the current method provides us a useful alternative in tailoring inorganic materials, noting that the method is simple and easy to operate. For restructuring catalytic materials, the technological merits of this method will be further addressed below:

(i) A thermally treated α-MoO_3 crystallite has a spatial dimension of [001] > [100] > [010]. This dimension order has been reversed by the current chemical etching, as evidenced in the etch pits shown in Figure 6d whose dimensional sequence is [100] > [001] > [010]. Since the chemical bonding situations of Mo−O on different crystallographic planes are very different, as discussed in the previous section, their coordinating properties to adsorbed species are different, i.e., catalytic performance may change.

(ii) In addition to the reversed order of dimensional changes, overall plane areas of both {001} and {100} are significantly increased due to internal etching while that of {010} is kept essentially the same. The etching will provide an overall increase in surface area and thus more active sites for a specific reaction.

(iii) Although chemically stabilized planes are {010}, {001}, and {100} upon etching, wavy etching fronts can also be fabricated which has been shown in Figure 5c and Figure 6b−d. Since chemical etching is in atomic level, the irregular etching fronts contain more atomistic defects that may provide more catalytically active sites for certain reactions.

(iv) With this method, it is possible to engineer microsteps, ledges, and terraces composed of a combination of either {100} and {010} or {001} and {010}. Unlike the singular plane situation of calcined α-MoO_3 catalysts, these *alternate* crystallographic planes (crystal edges and slopes or walls in the etch pits, Figure 7) obtained may be necessary for certain chemical reactions.

(v) Using this method, the α-MoO_3 is prepared at high temperatures while its surface structure is chemically carved at low temperature; the unique process may create unique structure/

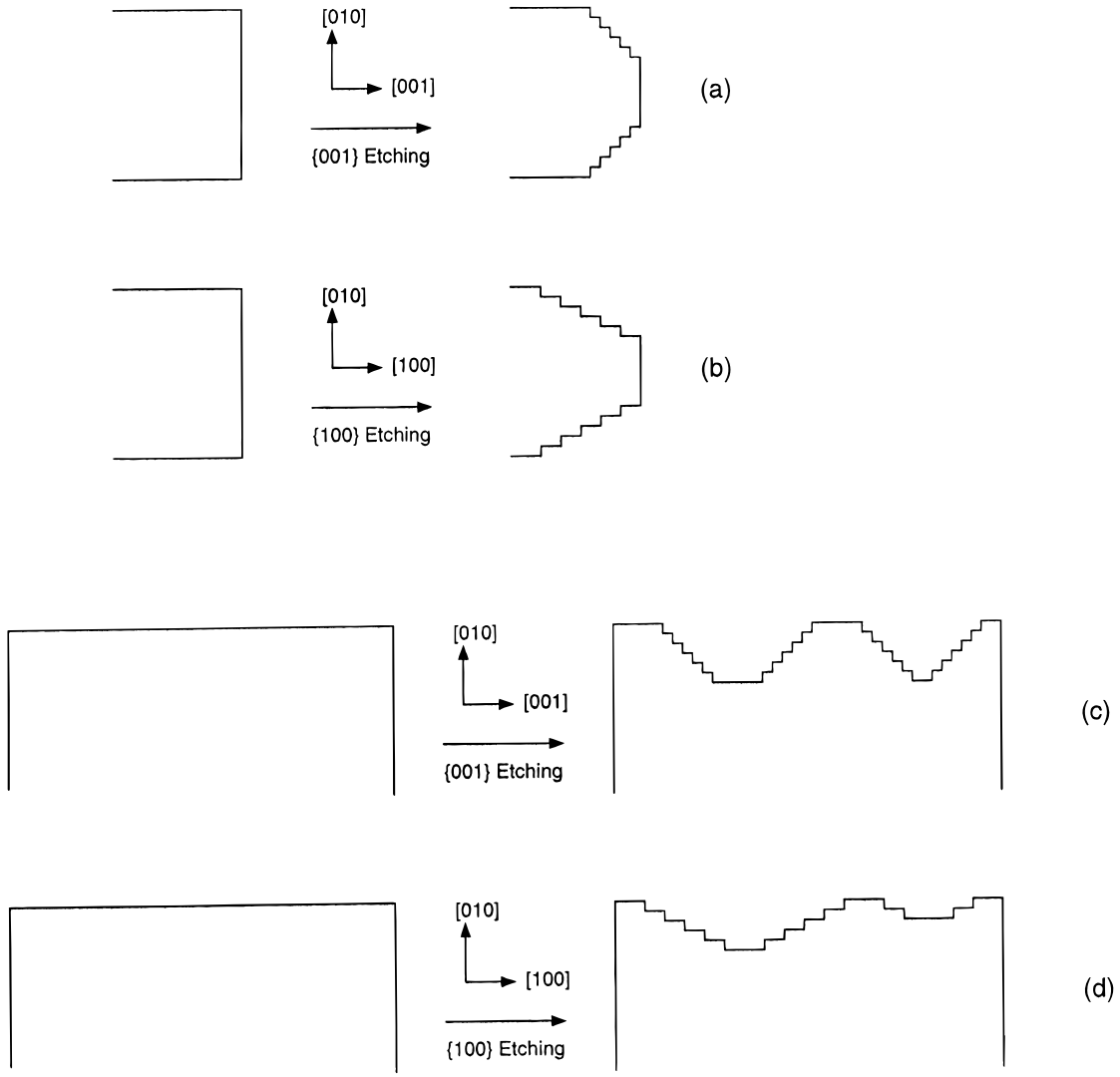

Figure 7. Schematic drawings of the chemical etchings on MoO_3 catalysts: (a) external {001} etching, (b) external {100} etching, (c) internal {001} etching, and (d) internal {100} etching.

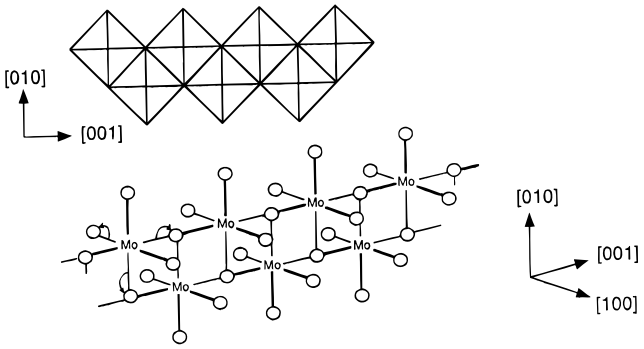

Figure 8. Proposed chain-peeling mechanism and relevant crystallographic orientations in {100} face etching; thin lines indicate bonds to be broken (as illustrated by arrows), while thick lines denote the Mo−O bonds that will be formed in MoO_4^{2-} after chemical etching.

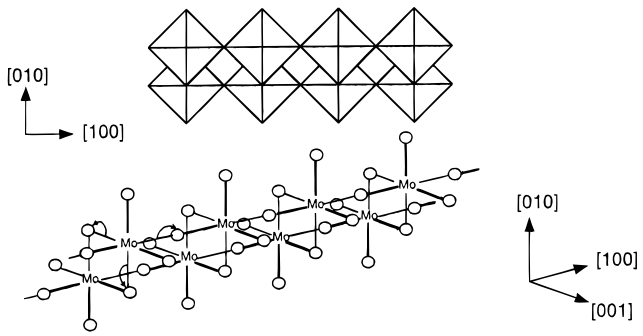

Figure 9. Proposed chain-peeling mechanism and relevant crystallographic orientations in {001} face etching; thin lines indicate bonds to be broken (as illustrated by arrows), while thick lines denote the Mo−O bonds that will be formed in MoO_4^{2-} after chemical etching.

active sites that a high temperature prepared phase does not possess. As long as the operating temperature of catalyst is not too high, these thermodynamically metastable surface phases will survive through the reactions.

(vi) The fabrication of these active sites and structures can be kinetically controlled by varying the concentration of NaOH, etching time, and temperature. Many processing parameters can be tested and selected in association with an actual catalytic chemical reaction of interest.

V. Conclusions

From fundamental viewpoint, we have looked at the materials chemistry between the solid MoO_3 and NaOH etchant in this study. The full impact of this chemically restructured MoO_3 on heterogeneous catalytic applications will only be seen when

all MoO_3-involving chemical reactions have been tested. Further experimental investigations on these chemical reactions are urgently needed, although they are apparently not a simple task.

In summary, vapor phase prepared α-MoO_3 catalysts have be studied with XRD, FTIR, and chemical etching methods. Using the NaOH etchant, it has been revealed that the {001} and {100} planes of catalysts are significantly increased upon the etching. In particular, the increase in {001} surface is more than that of the {100}, while the {010} remains essentially the same. Moreover, arising from this etching, alternate crystal plane combinations of either {100} and {010}, or the {001} and {010} are observed on the crystal edges and rectangular etch pits in the basal planes {010}. Surface steps, ledges, and terraces are also created by the low-temperature etching. Chemical interaction of MoO_3 and the etchant has been studied and etching mechanisms have been proposed based on the surface morphological evolution and formal charge consideration. Based on the experimental results of the current work, it is suggested that the chemically carved surface structures may be important for certain MoO_3-involving catalytic reactions. Methodological merits and the processing parameters have also been discussed.

Acknowledgment. The author gratefully acknowledges the research funding (RP960716) co-supported by the Ministry of Education and the National Science and Technology Board of Singapore and the technical assistance provided by Ms. H. C. Hia and Mr. C. W. Sheu.

IC971269V